WARSAW UNIVERSITY OF TECHNOLOGY Index 351733
FACULTY OF CIVIL ENGINEERING
COMMITTEE FOR CIVIL AND WATER ENGINEERING
POLISH ACADEMY OF SCIENCES ISSN 1230-2945

DOI: 10.24425/ace.2026.1389

ARCHIVES OF CIVIL ENGINEERING

Vol. LXXII ISSUE 3 2026

 pp. 285 – 300

Research paper

Ultimate strength estimation of short thin-walled cold-formed steel lipped channel section members under eccentric compression loads using yield line analysis

Jacek Jankowski[1], Leszek Czechowski[2], Maria Kotełko[3], Viorel Ungureanu[4], Annabella Sanduly[5]

Abstract: The paper presents findings from an analytical-numerical investigation on the use of yield line analysis (YLA) for the upper bound estimation of the ultimate strength of short thin-walled cold-formed steel (TWCFS) lipped channel section members under eccentric compression loads around both the minor and major axes. The post-buckling paths are analysed using the finite difference method (FDM). The post-ultimate failure curves are developed through theoretical models of plastic mechanisms, based on experimental tests and finite element (FE) simulations. The methodology presents the results in terms of load-shortening, alongside comparative diagrams of ultimate strength relative to eccentricity. The ultimate strength is assessed through the estimation of the upper bound using YLA, finite element analysis, experimental testing, and predictions based on the EN 1993-1-3 standard. Conclusions regarding the potential application of upper bound ultimate strength estimation using the YLA approach are drawn, along with discussions on the challenges of implementation and suggestions for future research in this area.

Keywords: cold-formed steel members, eccentric compression, ultimate strength, yield line analysis

[1]PhD., Eng., Lodz University of Technology, Faculty of Mechanical Engineering, Stefanowskiego 1/15 St., 90-537 Lodz, Poland, e-mail: jacek.jankowski@p.lodz.pl, ORCID: 0000-0002-9628-2799
[2]DSc, Eng., Lodz University of Technology, Faculty of Mechanical Engineering, Stefanowskiego 1/15 St., 90-537 Lodz, Poland, e-mail: leszek.czechowski@p.lodz.pl, ORCID: 0000-0002-4718-6215
[3]Professor, DSc, PhD., Eng., Lodz University of Technology, Faculty of Mechanical Engineering, Stefanowskiego 1/15 St., 90-537 Lodz, Poland, e-mail: maria.kotelko@p.lodz.pl, ORCID: 0000-0001-7784-4349
[4]Prof., DSc, PhD., Eng., Department of Steel Structures and Structural Mechanics, Politehnica University of Timisoara, e-mail: viorel.ungureanu@upt.ro, ORCID: 0000-0002-5826-9518
[5]PhD Student, Lodz University of Technology, Faculty of Mechanical Engineering, Stefanowskiego 1/15 St., 90-537 Lodz, Poland, e-mail: annabella.sanduly@dokt.p.lodz.pl, ORCID: 0000-0003-0568-3181

1. Introduction

Thin-walled cold-formed steel (TWCFS) members are widely used in the construction industry because of their favorable properties. Nowadays, a multiplicity of widely different products, with a tremendous diversity of shapes, sizes, and applications are produced in steel using the cold-forming process. The range of use of cold-formed steel sections specifically as load-bearing structural components is very wide, encompassing the building and automobile industry, shipbuilding, rail transport, the aircraft industry and many others. In the building sector, TWCFS structural elements have traditionally been employed as secondary load-carrying members in a wide range of applications, such as roof purlins, wall girts, stud walls and cladding. In a more recent trend, TWCFS structural elements are also increasingly being used as primary structural members, especially in low- to mid-rise multi-storey buildings and portal frames with short to intermediate spans. Thin-walled cold-formed steel (TWCFS) short members are susceptible to premature local or distortional buckling and lack significant post- elastic capacity. Multiple local buckling modes can occur simultaneously under the same critical load, with the possibility to interact, and their failure resulting in a localised plastic mechanism. This represents the first form of interaction and leads to unstable post-critical behaviour. Consequently, its collapse, whether in compression or bending, is transforming into a spatial plastic failure mechanism. For longer members, this represents the first form of interaction. As a result, the interactive local-global buckling is of a plastic-elastic nature [1]. They are also widely used in storage rack systems (frames). In this context, alternative methods for predicting the ultimate strength are essential, focusing on collapse behaviour, unlike traditional approaches such as the effective width method or the Direct Strength Method, recommended (among others) by AISI [2]. Such an approach is Yield Line Analysis (YLA), which can be applied to analyze the behaviour near the ultimate load and in the post-ultimate stage of TWCFS members. The point where the elastic post- buckling path intersects with the post-ultimate failure curve of the mechanism (see Fig. 1) offers an upper bound estimate of the load carrying capacity (ultimate strength) of the member [3].

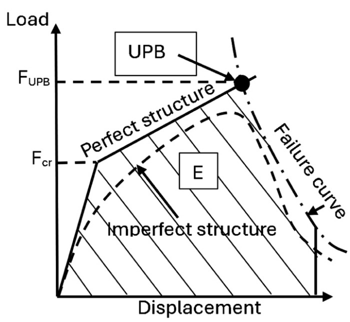

Fig. 1. Equilibrium path of thin-walled member

Thus, the usage of post-buckling elastic path for perfect structure combined with the post-ultimate curve (failure curve) provides an information about the upper bound point corresponding to FUPB. It makes the YLA approach attractive for the performance-based design of thin-walled structures. The issue of determining the load carrying capacity of the TWCFS under simple loading conditions (pure bending or uniform compression) has been addressed with satisfactory precision using thin-walled structure theory and design code specifications. EN 1993-1-3 [4] offers reliable predictions for the buckling load and ultimate strength of TWCFS members under concentric axial compression but is less precise for eccentrically compressed columns. In such cases, it is worth examining the applicability of the YLA approach, which provides an upper bound estimate of the ultimate strength. Bakker [5] categorised the yield line analysis (YLA) into two approaches: classical and generalised. Classical YLA focuses mainly on determining the load capacity of reinforced concrete structural members. It assumes that only primary bending moments contribute to the plastic strain energy dissipated within the plastic mechanism. The origins of classical YLA date back to the early 20th century, with fundamental contributions from Ingerslev in 1923 [6], Rzanicyn in 1949 [7], and Sawczuk and Jaeger in 1963 [8]. These studies addressed the analysis of plastic mechanisms (yield line theory) to estimate the load capacity of reinforced concrete plates and slabs. Although classical YLA remains part of concrete design specifications, it cannot be applied directly to analyse the structural behaviour of TWCFS members. Generalized yield line analysis provides a load-deformation post-ultimate relationship by deriving the plastic strain energy dissipated in the spatial mechanism due to second-order displacement fields. This approach was first applied in the 1970s to analyse the post-ultimate behavior of TWCFS members. The first applications in metal structures were reported by Murray in 1975 [9]. Pioneering efforts were continued by Murray and Khoo [10], Mahendran [11], and Rasmussen and Hancock [12], who investigated local plastic mechanisms in channel section columns and thin-walled plates under compression. Since then, extensive research has focused on spatial plastic mechanism analysis to evaluate the ultimate and post-ultimate behaviour of TWCFS members. More recently, YLA has been applied to analyse failure mechanisms and post-ultimate behaviour of corrugated plate structures by Timmers [13] and Casariego et al. [14]. Kobashi et al. [15] used YLA to study strength deterioration in relatively long channel section columns under compression. Segura et al. [16] introduced a new plastic mechanism model, based on finite element simulations and experiments, which facilitated the derivation of moment-rotation relationships for tubular T-joints in steel and stainless steel structures. Furthermore, Kotełko et al. [17] used YLA to estimate the ultimate strength of perforated lipped channel section columns under compression. Research on the structural behaviour of TWCFS members under eccentric compression, particularly in relation to the channel section members and (particularly) subject to major axis bending, remains relatively limited. A comprehensive state-of-the-art review in this field is provided in [18–20]. He et al. [21] examined built-up (back-to-back) section members with V- or Σ-shaped web stiffeners subjected to both concentric and eccentric compression using the Finite Element Method (FEM), which was validated against experimental results. Zhao et al. [22] reported strength predictions based on the Direct Strength Method (DSM) and compared them to experimental test results for perforated TWCFS channel section members under eccentric compression. In [23], the structural behaviour of eccentrically loaded TWCFS beam-columns with lipped and sigma channel sections was studied experimentally and analytically under the combined effects of axial loads and biaxial bending moments. Shuhao and Papangelis [24] investigated the distortional buckling of cold-formed steel channels bent about the minor axis with the lips in compression. They compared the ultimate moments calculated by the non-linear finite element analysis with the current DSM design equations and presented a new DSM design equation. Some papers published recently are devoted to I-sections under combined load. Weber et al. [25] investigated I-section stub columns with different cross-section profiles subjected to axial compression as well as I-section specimens subjected to combined compression and bending, printed via WAAM using high strength steel grade ER90S-G welding wire. The combined loading specimens achieved resistances surpassing the Eurocode 3 (EC3) predictions, but were prone to tensile fracture at large loading eccentricities. Feber et al. [26] performed the experimental and numerical investigations of austenitic stainless steel I-section beam-columns submitted to compression and major axis bending failing by major axis flexural buckling. The experimental part consisted in beam-column tests, with varied loading eccentricities providing a wide range of major axis bending moment-to-axial load (M/N) ratios. The results of the parametric study were compared with the existing design rules. The problem of eccentric compression of back-to-back built up sections with web stiffeners under axial and eccentric compression was also analysed by Schafer et al. [27], who presented new experimental results comprising built-up sections with V-stiffeners and with Σ-stiffeners of different member lengths under the axial and eccentric compression loading to reveal the potential failures and load-carrying capacity of these built-up sections. The experimental results provided the details of the buckling behavior and failure modes and a set of load response curves. Tubular steel corroded members under eccentric load were studied by Thong M. Pham et al. [28]. Huang and Zhang [29] studied a high-strength steel welded I-section overall buckling performance under axial compression and bending with respect to the major axis. The findings of the studies mentioned above suggest that the design rules in the existing standards for TWCFS members under eccentric compression are overly conservative and require improvement, particularly in terms of interactive formulae for combined compression and bending. Subsequent research by the authors of [20, 30] further explored this topic through experimental programs and theoretical analyses of short members with lipped channel cross-sections subjected to eccentric compression about both the minor and major axes across a wide range of eccentricities. The post-ultimate rigid-plastic curves, the characterizing post-ultimate structural behaviour and derived using plastic mechanism models, were compared with experimental and FE simulation results. This paper builds on the research aforementioned by applying the Yield Line Analysis (YLA) method to estimate the ultimate strength of lipped channel cross-section short columns subjected to eccentric compression about the minor and major axes.

2. Scope and objectives of analysis

This study focuses on the structural behaviour of TWCFS lipped channel columns under eccentric compression around both the minor and the major axes (Fig. 2). The dimensions of the columns (Fig. 2, on the right) were selected to ensure they fall into class 4 [31], indicating that local buckling occurs in these members before any part of the cross-section reaches yield stress, according to the standard classification [4].

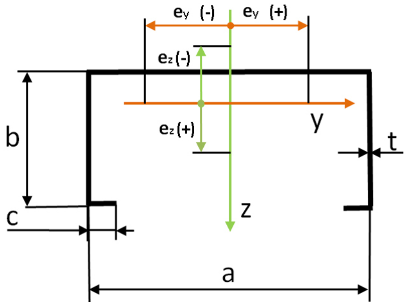

No.	a (mm)	b (mm)	c (mm)	t (mm)	l (mm)
1	150	60	20	2	450
2	150	60	20	1	450
3	150	47	16	2	450
4	150	47	16	1.5	450
5	150	47	16	1	450
Internal radii: r = 1.5 mm (for t = 1 mm) and r = 2.5 mm (for t = 2, 2.5 mm)					

Fig. 2. Lipped channel section (with dimension) subject to minor/major axes eccentric compression

An extensive research program was conducted, including both theoretical analysis and experimental investigation, to explore the structural behaviour (including post-ultimate behaviour) of TWCFS lipped channel columns under eccentric compression about the minor and major axes. The findings of this research have been presented in [18–20]. The structural behaviour of the members was analysed theoretically using the Finite Difference Method (FDM), Finite Element (FE) simulations, and the Yield Line Analysis (YLA) method, as well as experimentally tested for a wide range of eccentricities, i.e. from –60 mm to +60 mm about the minor axis and from 0 to 60 mm about the major axis. The objectives of this study are the following:

1) to analyze the post-buckling elastic behaviour of the members, focusing on the applicability of post-buckling paths for upper-bound estimation of the load-carrying capacity of the investigated members,
2) to predict the upper-bound ultimate strength based on post-buckling FDM analysis and the YLA method.

3. Methodology

As already mentioned, estimating the upper bound load capacity requires determining the ordinate of the intersection point between the post-buckling curve and the post-ultimate mechanism failure curve. The following sections describe the methodology used to analyse these segments of the load-displacement path of the members. These paths obtained by the described methods are compared with the results of the FE simulations and the experimental data [18–20].

3.1. Pre- and post-buckling analysis

To investigate the nonlinear behaviour of thin-walled members, particularly in the post-buckling state, the strain tensor components, constitutive relations, continuity equations (between the two walls of the member section), and equilibrium equations were formulated. The system of two plates is described using continuity equations [32] that were taken into account in further analysis with FDM. For each thin plate, the nonlinear strain-displacement relations were defined based on Timoshenko's approach [32]. The constitutive linear relations (generalised Hooke's law) for isotropic materials were assumed. The internal in-plane forces and moments (bending moments and torque) were derived from the classical first-order theory of thin plates [32]. The equilibrium equations were obtained by applying the principle of potential energy variation formulated for a single.

The resulting simultaneous nonlinear algebraic equation, derived from the differentiating equations, was computed using the one-step Newton-Raphson method. This approach accounts for both global and local buckling modes. Furthermore, the continuity equations between plates were considered (though not detailed in this paper). The boundary conditions for the analysed simply supported structure were expressed in terms of sectional forces and kinematic conditions [33]. The discretization of the equilibrium equations leads to mapping for each wall. To address the buckling and post-buckling problems, boundary conditions were considered separately for eccentricity about the major and minor axes. For the buckling problem, linear boundary conditions were applied for small displacements. However, for the post-buckling problem, nonlinear boundary conditions were used due to the occurrence of large displacements. The boundary conditions, expressed through difference quotients, are defined at the two edges of the lips, the two edges of the flanges, and the two edges of the web of the analysed member, which is simply supported at both ends. A detailed description of the boundary conditions expressed by the difference quotients can be found in [33].

3.2. Yield-line analysis

The YLA assumes that deformations leading to the formation of failure plastic mechanisms are concentrated along zero-width yield lines. The assumption is that the plastic mechanism is fully developed, with plastic zones in the walls of thin-walled steel members concentrated in the yield lines, which can be stationary or travelling [20]. At the yield line level, the material is considered to be entirely plastic. The material properties are assumed to be either rigid-perfectly plastic or rigid-plastic with strain hardening. The theory distinguishes two types of plastic mechanisms: the "true mechanism" and the "quasi-mechanism", where the flat sections of the walls are limited by yield lines, but the walls still undergo membrane deformation. The plastic mechanism approach is based on two methods: the energy method (work method) and the equilibrium strip method [9, 10]. In this study, only the energy method is used. When the energy method is applied, the Principle of Virtual Velocities is used. For TWCFS members, the following form of this principle, related to the rate of change in the energy dissipated, is typically employed, Eq. (3.1), where $\dot{\Pi}$ is the potential energy of the system.

$$\dot{\Pi}(\dot{\beta}, \chi) = \sum_i \int_{A_i} (N_0 \varepsilon_p) dA_i + \sum_j \dot{E}_{bj}(\dot{\beta}_j, \overline{m}_{pj} \chi) \tag{3.1}$$

Equation (3.1) represents the sum of the rate of change in the membrane strain energy within the walls of the global plastic hinge and the bending strain energy dissipated in the yield lines, where N_0 is a vector of membrane forces per unit length. The membrane forces N_0 are determined using the associated flow rule, based on the corresponding yield criterion (e.g., Huber–Mises). A_i refers to the area of the i-th plastic zone (tension field), $\dot{\beta}_i$ is the angular velocity vector on the i-th yield line, ε_p is the plastic strain tensor, χ is the vector of independent geometric parameters that describe plastic mechanism, and $\overline{m}_{pi}$ is the plastic moment vector along that line. The first component of Eq. (3.1) is considered only in the case of quasi-mechanisms, which include both yield lines and plastic zones (tension fields). For the true mechanism, only the second component of Eq. (3.1) should be taken into account, where E_{bi} represents the bending strain energy dissipated at the i-th yield line. This relation is usually rearranged into the following form (3.2):

$$\delta W_{\text{ext}} = \delta E_b + \delta E_m \tag{3.2}$$

δW_{ext} is the variation in the work of external forces, δE_b is the variation in the bending plastic deformation energy, and δE_m is the variation in the membrane plastic deformation energy. Equation (3.2) establishes a relationship between the generalised load (e.g., compressive load, bending moment) and the generalised displacement (e.g., shortening, angle of rotation). The graphical representation of this relationship is the failure (post-ultimate) curve. The plastic moment vector $\overline{m}_{pi}$ at yield lines perpendicular to the load direction is expressed as a full plastic moment using the relation (3.3):

$$m_p = \frac{\sigma_y \cdot t^2}{4} \tag{3.3}$$

However, in the case of yield lines inclined to the load direction (referred to as *inclined yield lines*), the plastic moment is reduced due to the combined effects of membrane forces, shear forces, and twisting moments. Various researchers have proposed different formulas to calculate the plastic moment capacity in inclined yield lines [3, 34], with significant variations depending on the stress distribution under fully plastic conditions at these inclined yield lines. Since a spatial collapse mechanism involves multiple inclined yield lines, the predicted failure (post-ultimate) curve is influenced by the assumed stress distribution model at these lines and the corresponding formulas for the plastic moment vector. Zhao and Hancock have extensively described this issue in their studies [35, 36].

Three selected stress distribution models at the yield line are illustrated in Fig. 3. The first model (Fig. 3a) represents the full plastic moment. The Murray model (Fig. 3b) accounts for the reduction in plastic moment capacity due to the interaction of axial force and bending moment, while neglecting shear stresses in the yield line cross-section [37]. As a result, the plastic moment capacity is expressed as Eq. (3.4). Murray provided further clarification in the model shown in Fig. 3c [38].

$$m = m_p \left[1 - \left(\sigma/\sigma_{pl}\right)^2 \cdot \cos^4 \gamma\right] \tag{3.4}$$

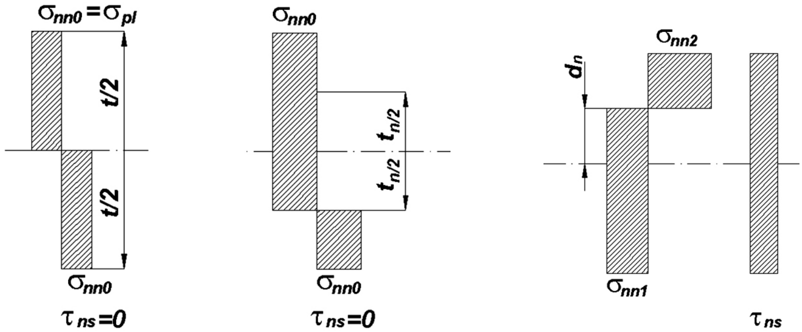

(a) (b) (c)

Fig. 3. Stress distribution in the yield line cross-section: (a) fully plastic moment, (b) Murray model (1973) [37], (c) Murray model (1984) [38]

This model incorporates uniformly distributed shear stresses in the cross- section of the yield line inclined in the principal direction. Based on the Huber–Mises yield criterion, the plastic moment capacity in this case is expressed as Eq. (3.5).

$$m = m_p \frac{\left[1 - \left(\sigma/\sigma_{pl}\right)^2\right]}{\sqrt{1 - 0.75\left(\frac{\sigma}{\sigma_{pl}}\right)^2 \sin^2\gamma\left[\sin^2\gamma + 4\left(1 - \sin^2\gamma\right)\right]}} \tag{3.5}$$

In this paper, the fully plastic moment, together with Eq. (3.4) and Eq. (3.5) were considered to investigate the influence of the stress distribution model at the applied yield line. The normal stress σ, which corresponds to the stress induced by the axial force, was assumed to be equal to the buckling stress obtained from the FDM analysis [33]. For the examined members and eccentricities, the ratio σ/σ_{cr} is approximately 0.7–0.8. According to the analysis by Hiriyur and Schafer [3], in this range of the ratio, the reduction in plastic moment capacity for both Murray models is approximately 10% for a 40° inclined yield line to the principal direction.

4. Plastic mechanism database

The key aspect of the YLA approach, as well as its main challenge, lies in accurately identifying yield line patterns and tension fields. This involves establishing the geometry of the spatial plastic mechanism and understanding how the mechanism evolves. This identification is achieved through experiments and FE simulations. Once an initial model of the mechanism is developed, its geometric parameters require detailed calibration [19]. In this paper, a database of plastic mechanisms created from previous research was used [18,20]. The theoretical models of these plastic mechanisms were largely derived from experimental data [19,20]. The experimental setup is depicted in Fig. 4, where failed components were scanned using 3D scanning technology, and the initially developed theoretical models were subsequently calibrated.

(a) (b)

Fig. 4. Experimental stand: eccentricity about minor axis (a) and eccentricity about major axis (b) [19]

The calibration process is illustrated in Fig. 5. This calibration process helps in refining the geometry of the theoretical model.

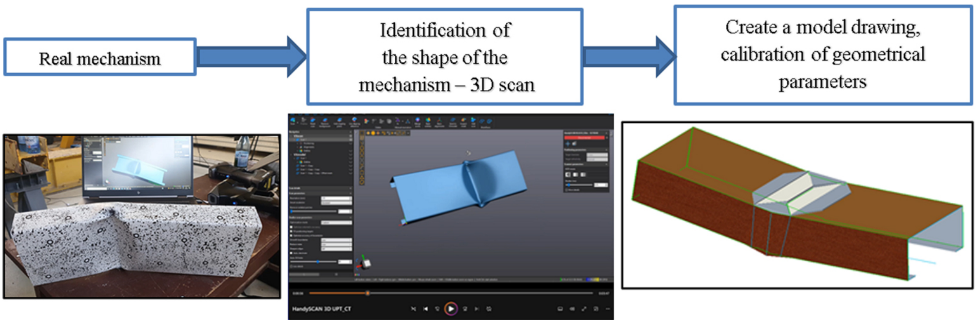

Fig. 5. Calibration example of the theoretical mechanisms for a member in eccentric compression around the major axis [20]

The authors developed models and analytical formulations for plastic mechanisms in two accompanying papers [18, 19], with the aim of characterising the post-ultimate strength of members subjected to eccentric compression around the minor axis.

Based on experimental observations and FE numerical results, five plastic mechanism models were validated for the eccentricities about minor axis (Fig. 6).

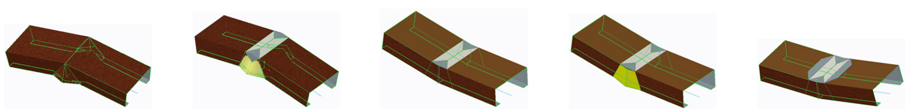

(a) (b) (c) (d) (e)

Fig. 6. Plastic mechanism models for various eccentricities about minor axis: (a) CF1 (small positive “e”), (b) CFQ (medium and large positive “e”), (c) pitched roof – (small negative “e”), (d) Pitched roof I (medium and large negative “e”), (e) (very large negative “e”)

These models were calibrated, and the post-ultimate mechanism curves derived using YLA showed a strong correlation with FE simulations and experimental findings [19]. Furthermore, two theoretical models for plastic collapse mechanisms were created for members subjected to eccentric compression about the major axis [30], based on experimental and FE results (see Fig. 7).

Fig. 7. Plastic mechanism models for various eccentricities about major axis: axis: (a) "V" (e = 0–30 mm), (b) "W" (e > 30 mm)

In this scenario, the post-ultimate curves derived from the "V" model aligned more closely for eccentricities between 0 and 30 mm and wall thicknesses of 1 mm and 1.5 mm. In contrast, the mechanism curves derived from the "W" model better described eccentricities greater than 30 mm and wall thicknesses of 1.5 mm and 2 mm. In the subsequent upper-bound estimate of the load capacity of the examined members, both mechanism models were incorporated.

5. Results of upper bound estimate of load capacity

5.1. Load- displacement paths

Using the methodology presented in the first part of the paper, load- displacement paths for the members under investigation were developed for the entire loading range, extending beyond the ultimate load. These paths were compared with experimental and finite element results. Sample diagrams illustrating the load-shortening paths of members subjected to eccentric compression about the minor axis are presented in Fig. 8.

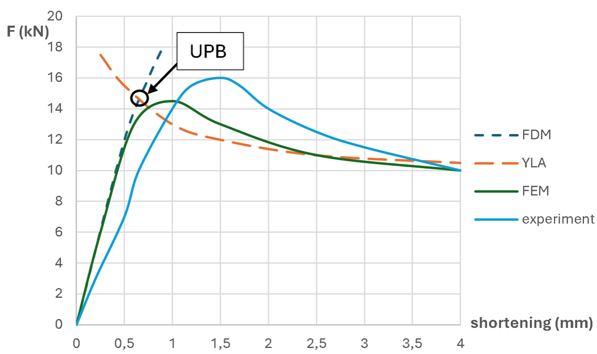

Fig. 8. Load-shortening path for 150 × 60 × 20 × 1 mm lipped channel specimen, e = −40 mm (minor axis), YLA – mechanism "Pitched Roof I"; fully plastic moment

Similar diagrams showing the load-shortening paths of the member under eccentric compression along the major axis are presented in Fig. 9.

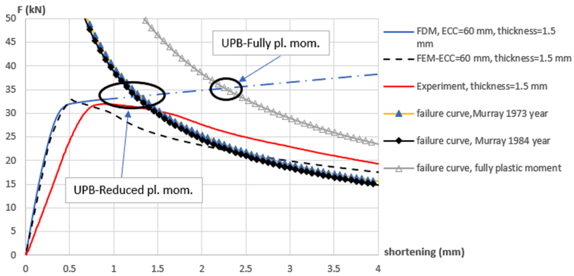

Fig. 9. Load-shortening path for 150 × 47 × 16 × 1.5 mm lipped channel specimen, e = 60 mm (major axis), YLA – mechanisms "W"

In this diagram, the post-ultimate, failure curves relate to the mechanism model "W". Three mechanism curves are shown, derived from the equations corresponding to the full plastic moment capacity (3.3) and the reduced plastic moment capacity from Eq. (3.4) and Eq. (3.5), along with an upper- bound load capacity estimation. As underlined, while the reduction in plastic moment capacity does not have a significant effect on the upper bound load capacity, the positioning of the post-ultimate curves varies considerably. Consequently, in further evaluations of the upper bound load capacity estimation, the fully plastic moment capacity was considered.

5.2. Ultimate strength – comparison of results

The ultimate strength of the studied members was assessed using the upper bound approach, incorporating post-buckling and post-ultimate YL analyses. The upper-bound estimates were compared with experimental results, finite element (FE) analyses, and standard predictions [2]. The comparative diagrams illustrating ultimate strength versus eccentricity for members subjected to eccentricity about the minor axis are presented in Fig. 10 and Fig. 11.

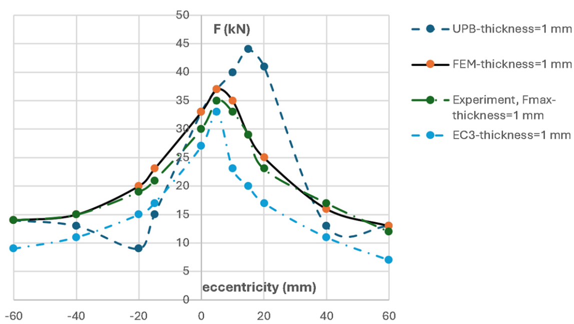

Fig. 10. Ultimate strength versus eccentricity about minor axis for 150 × 60 × 20 × 1 mm lipped channel specimen

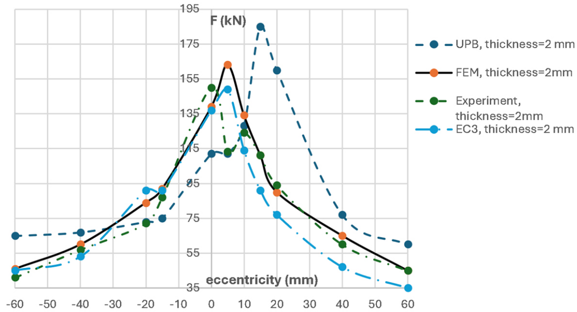

Fig. 11. Ultimate strength versus eccentricity about minor axis for 150 × 60 × 20 × 2 mm lipped channel specimen

Similarly, Fig. 12, Fig. 13 and Fig. 14 show comparative diagrams of ultimate strength for members subjected to eccentricity around the major axis for t = 1 mm, 1.5 mm and 2 mm, respectively.

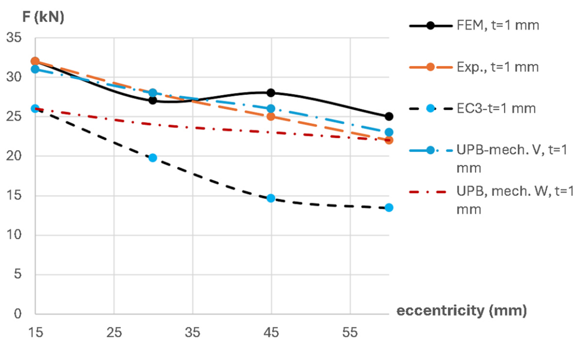

Fig. 12. Ultimate strength versus eccentricity about major axis for 150 × 60 × 20 mm lipped channel specimen for t = 1 mm

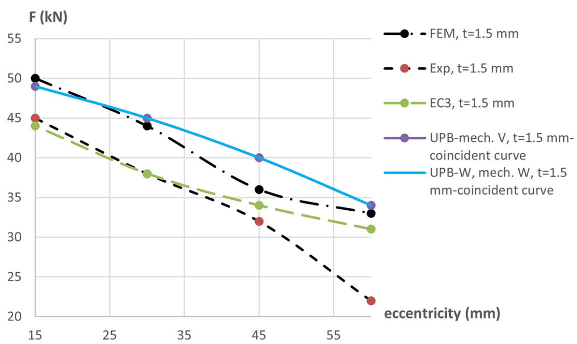

Fig. 13. Ultimate strength versus eccentricity about major axis for 150 × 60 × 20 mm lipped channel specimen for t = 1.5 mm

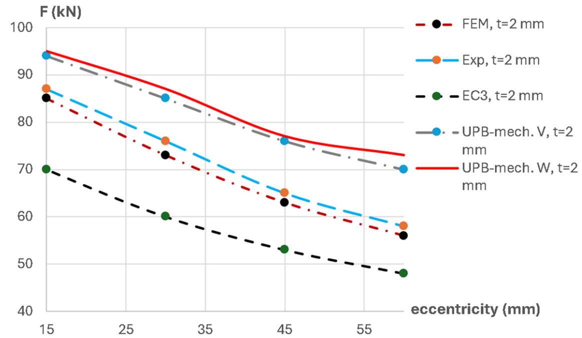

Fig. 14. Ultimate strength versus eccentricity about major axis for 150 × 60 × 20 mm lipped channel specimen for $t = 2$ mm

Figures 15 and 16 present the comparative diagrams of the ultimate strength under eccentric compression on both the minor and major axes for the entire range of eccentricities and all tested members.

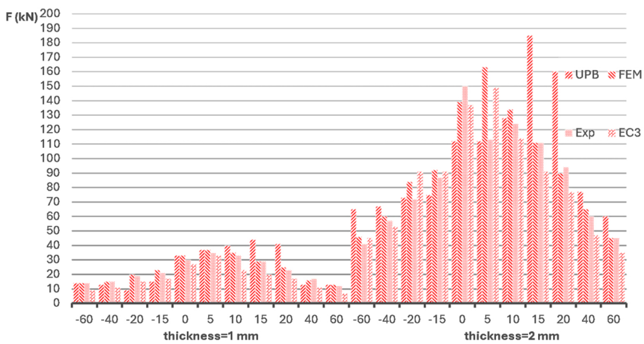

Fig. 15. Comparative results for 150 × 60 × 20 mm lipped channel specimen with $t = 1$ mm and $t = 2$ mm. Ultimate strength versus eccentricity about minor axis

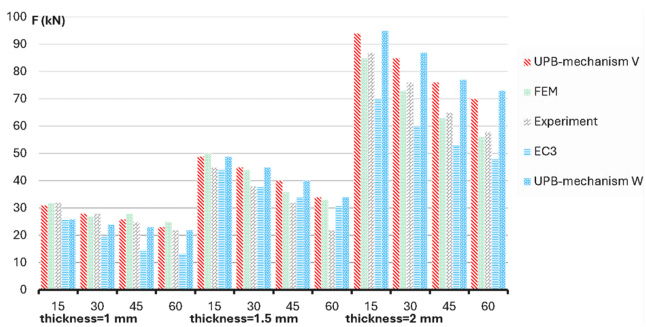

Fig. 16. Comparative results for 150 × 60 × 20 mm lipped channel specimen with $t = 1$ mm, $t = 1.5$ mm and $t = 2$ mm. Ultimate strength versus eccentricity about major axis ("V" vs. "W" mechanism)

6. Conclusions and final remarks

This paper presents an analytical-numerical study on the application of the YLA method for upper bound estimation (UPB) of ultimate strength in short TWCFS lipped channel section members subjected to eccentric compression about both minor and major axes. The results obtained validate the use of the YLA approach, along with pre- and post-buckling analyses, to assess the load carrying capacity of the investigated members. For members subjected to eccentric compression about the minor axis with a wall thickness of 1 mm, there is satisfactory agreement between the upper bound prediction, finite element (FE) and experimental results, with the lowest relative discrepancy being less than 1%. However, this agreement increases with increasing wall thickness. The largest discrepancy between UPB and both FE simulations and experimental results for members of both wall thicknesses occurs at a positive eccentricity of approximately 20 mm, which corresponds to the maximum ultimate load. For the major axis, satisfactory agreement between UPB, FE, and experimental results was observed for wall thicknesses of 1 mm and 1.5 mm. On the contrary, for members with the greatest wall thickness of 2 mm, the upper bound estimation does not fully align with FE and the experimental results. The UPB estimation derived from both theoretical models applied, "V" and "W", produces very similar outcomes.

These findings highlight the need for further refinement of theoretical plastic mechanism models, especially for positive eccentricities near the maximum ultimate load and across the full range of positive and negative eccentricities for column height to wall thickness ratios below 100. Standard predictions of ultimate strength for the examined cases (members under eccentric compression, involving combined compression and bending) are conservative compared to FE simulations and experimental values across the entire range of tested eccentricities. Therefore, the UPB ultimate strength prediction method using the YLA approach discussed in this study is promising. Ongoing research aims to enhance this method, particularly by refining theoretical models of plastic mechanisms and developing relatively simple algorithms for UPB evaluation.

Acknowledgements

This work was supported by a grant 2019/35/B/ST8/02823 – Implementation of yield line theory to the load-capacity estimation of thin-walled members under combined load, of the National Science Centre of the Polish Ministry of Science and Higher Education.

References

[1] V. Ungureanu and D. Dubina, "Recent research advances on ECBL approach. Part I: Plastic-elastic interactive buckling of cold-formed steel sections", *Thin-Walled Structures*, vol. 42, no. 2, pp. 177–194, 2004, doi: 10.1016/S0263-8231(03)00056-9.

[2] AISI S100-16 North American Specification for the Design of Cold-Formed Steel Structural Members. American Iron and Steel Institute, 2016.

[3] B.K.J. Hiriyur and B.W. Schafer, "Yield-line analysis of cold formed steel members", *International Journal of Steel Structures*, vol. 5, pp. 43–54, 2005.

[4] EN 1993-1-3 Eurocode 3: Design of Steel Structures, Part 1.3: General Rules, Supplementary Rules for Cold-formed Thin Gauge Members and Sheeting. CEN, 2006.

[5] M.C.M. Bakker, "Yield line analysis of post-collapse behavior of thin-walled steel members", *Heron*, vol. 35, no. 3, pp. 1–50, 1990.

[6] A. Ingerslev, "The strength of rectangular slabs", *Journal of Institution of Structural Engineers*, vol. 1, no. 1, pp. 3–14, 1923.

[7] A.R. Rzhanitsyn, *Plastic analysis of reinforcement in composite plates*. Moscow, 1949 (in Russian).

[8] A. Sawczuk and T. Jaeger, *Load-carrying capacity of plates*. Berlin: Springer, 1963 (in German).

[9] N.W. Murray, *Introduction to the theory of thin-walled structures*. Oxford: Clarendon Press, 1986.

[10] N.W. Murray and P.S. Khoo, "Some basic plastic mechanisms in the local buckling of thin-walled steel structures", *International Journal of Mechanical Sciences*, vol. 23, no. 12, pp. 703–713, 1981, doi: 10.1016/0020-7403(81)90008-4.

[11] M. Mahendran, "Local plastic mechanisms in thin steel plates under in-plane compression", *Thin-Walled Structures*, vol. 27, no. 3, pp. 245–261, 1997, doi: 10.1016/S0263-8231(96)00040-7.

[12] K.J.R. Rasmussen and G.J. Hancock, "Nonlinear analysis of thin-walled channel section columns", *Thin-Walled Structures*, vol. 13, no. 1-2, pp. 145–176, 1992, doi: 10.1016/0263-8231(92)90006-I.

[13] R. Timmers and G. Lener, "Collapse mechanisms and load-deflection curves of unstiffened and stiffened plated structures from bridge design", *Thin- Walled Structures*, vol. 106, pp. 448–458, 2016, doi: 10.1016/j.tws.2016.05.020.

[14] P. Casariego, M. Casafont, M. Ferrer, and F. Marimon, "Analytical study of flat and curved trapezoidal cold formed steel sheets by means of the yield line theory. Part 1: Flat sheets without transverse corrugations", *Thin-Walled Structures*, vol. 141, pp. 675–692, 2019, doi: 10.1016/j.tws.2018.12.017.

[15] T. Kobashi, "Evaluation of post-maximum strength behavior of lipped channel under compression", *Thin-Walled Structures*, vol. 180, art. no. 109939, 2022, doi: 10.1016/j.tws.2022.109939.

[16] G. Segura, I. Arrayago, and E. Mirabell, "New proposal for the bending moment capacity of tubular T-joints in carbon steel and stainless steel structures", *Thin-Walled Structures*, vol. 187, art. no. 110667, 2023, doi: 10.1016/j.tws.2023.110667.

[17] M. Kotełko, M. Macdonald, M.P. Kulatunga, and Z. Marszalek, "Upper bound estimation of load carrying capacity of perforated cold formed thin-walled steel lipped channel columns under compression loading", *Maintenance and Reliability*, vol. 21, no. 3, pp. 565–573, 2020, doi: 10.17531/ein.2020.3.20.

[18] M. Kotełko, J. Grudziecki, V. Ungureanu, and D. Dubina, "Ultimate and post- ultimate behaviour of thin-walled cold-formed steel open-section members under eccentric compression. Part I: Collapse mechanisms database (theoretical study)", *Thin-Walled Structures*, vol. 169, art. no. 108366, 2021, doi: 10.1016/j.tws.2021.108366.

[19] Ł. Borkowski, J. Grudziecki, M. Kotełko, V. Ungureanu, and D. Dubina, "Ultimate and post-ultimate behaviour of thin-walled cold-formed steel open- section members under eccentric compression. Part II: Experimental study", *Thin-Walled Structures*, vol. 171, art. no. 108802, 2022, doi: 10.1016/j.tws.2021.108802.

[20] V. Ungureanu, I. Both, M. Kotełko, L. Czechowski, F. Bodea, and D. Dubina, "Buckling strength and post-ultimate behaviour of lipped channel section short columns under eccentric compression", *Thin-Walled Structures*, vol. 181, art. no. 110085, 2022, doi: 10.1016/j.tws.2022.110085.

[21] Z. He, S. Peng, X. Zhou, Z. Li, G. Yang, and Z. Zhang, "Design recommendation of cold-formed steel built-up sections under concentric and eccentric compression", *Journal of Constructional Steel Research*, vol. 212, art. no. 108255, 2023, doi: 10.1016/j.jcsr.2023.108255.

[22] J. Zhao, J. He, B. Chen, W. Zhang, and S. Yu, "Test and direct strength method on slotted perforated cold-formed steel channels subjected to eccentric compression", *Engineering Structures*, vol. 285, art. no. 116082, 2023, doi: 10.1016/j.engstruct.2023.116082.

[23] F. Öztürk, S.M. Mojtabaei, M. Şentürk, S. Pul, and I. Hajirasouliha, "Buckling behaviour of cold-formed sigma and lipped channel beam-column members", *Thin-Walled Structures*, vol. 173, art. no. 108963, 2022, doi: 10.1016/j.tws.2022.108963.

[24] M. Shuhao and J. Papangelis, "Distortional buckling of cold-formed steel channels bent about the minor axis", *Thin-Walled Structures*, vol. 210, art. no. 112972, 2025, doi: 10.1016/j.tws.2025.112972.

[25] B. Weber, X. Meng, and L. Gardner, "Local buckling behavior of wire arc additively manufactured steel I-section under axial compression and combined loading", *Thin-Walled Structures*, vol. 211, art. no. 113027, 2025, doi: 10.1016/j.tws.2025.113027.

[26] N. Feber, M. Jandera, and B. Rossi, "Combined compression and bending of austenitic stainless steel I-section members", *Thin-Walled Structures*, vol. 209, art. no. 112819, 2025, doi: 10.1016/j.tws.2024.112819.

[27] Z. He, S. Peng, X. Zhou, G. Yang, and B.W. Schafer, "Failure characteristics of cold-formed steel built-up section with web stiffeners under axial and eccentric compression", *Thin-Walled Structures*, vol. 182, Part B, art. no. 110269, 2023, doi: 10.1016/j.tws.2022.110269.

[28] T.M. Pham, E.F. Ong, T.T. Tran, Y. Zhuge, K. Le-Nguyen, and L. Nguyen-Minh, "Compressive behavior of locally corroded steel tubular members under eccentric loads", *Thin-Walled Structures*, vol. 198, art. no. 111742, 2024, doi: 10.1016/j.tws.2024.111742.

[29] B. Huang and W.F. Zhang, "Overall buckling performance of high strength steel welded I-sections under combined axial compression and bending", *Archives of Civil Engineering*, vol. 68, no. 3, pp. 369–384, 2022, doi: 10.24425/ace.2022.141891.

[30] V. Ungureanu, M. Kotełko, F. Bodea, I. Both, and L. Czechowski, "Failure mechanisms of TWCFS members considering various eccentricities", *Steel Construction*, vol. 16, no. 1, pp. 44–55, 2023, doi: 10.1002/stco.202200045.

[31] EN 1993-1-1 Eurocode 3: Design of steel structures – Part 1-1: General rules and rules for buildings. CEN, 2005.

[32] S. Timoshenko and S. Woinovsky-Krieger, *Theory of plates and shells*. McGraw Hill Book Company, 1959.

[33] J. Jankowski, M. Kotełko, and V. Ungureanu, "Numerical and Experimental Analysis of Buckling and Post-Buckling Behaviour of TWCFS Lipped Channel Section Members Subjected to Eccentric Compression", *Materials*, vol. 17, no. 12, art. no. 2874, 2024, doi: 10.3390/ma17122874.

[34] M. Kotełko, "Load-capacity estimation and collapse analysis of thin-walled beams and columns – Recent advances", *Thin-Walled Structures*, vol. 42, no. 2, pp. 153–175, 2024, doi: 10.1016/S0263-8231(03)00055-7.

[35] X.L. Zhao and G.J. Hancock, "A theoretical analysis of the plastic moment capacity of an inclined yield line under axial force", *Thin-Walled Structures*, vol. 15, no. 3, pp. 185–207, 1993, doi: 10.1016/0263-8231(93)90026-7.

[36] X.L. Zhao and G.J. Hancock, "Experimental verification of the theory of plastic moment capacity of an inclined yield line under axial force", *Thin-Walled Structures*, vol. 15, no. 3, pp. 209–233, 1993, doi: 10.1016/0263-8231(93)90027-8.

[37] N.W. Murray, "Moment capacity at the yield line inclined to the normal force", *Die Bautechnik*, vol. 50, no. 2, pp. 57–58, 1973 (in German).

[38] N.W. Murray, "The effect of shear and normal stresses on the plastic moment capacity of inclined hinges in thin-walled steel structures", in *Festschrift Roik*. Bochum: Inst. fr Konstruktiven Ingenieurbau, Ruhr Univ. Bochum, 1984, pp. 237–248.

Szacowanie górnej granicy nośności dla cienkościennych zimno formowanych stalowych profili ceowych ściskanych mimośrodowo

Słowa kluczowe: zimno formowane profile cienkościenne, ściskanie mimośrodowe, nośność graniczna, plastyczny mechanizm, analiza krzywej plastycznej

Streszczenie:

Artykuł dotyczy wyników obliczeń analityczno- numerycznych w oparciu o analizę krzywej załomów plastycznych pozwalającą uzyskiwać górne szacowanie nośności krótkich i cienkościennych profili ceowych pod obciążeniem mimośrodowego ściskania. Ścieżki pokrytyczne były otrzymywane i analizowane w oparciu o metodę różnic skończonych. Krzywe zniszczenia w zakresie pokrytycznym były uzyskiwane dzięki teoretycznym modelom plastycznych mechanizmów z testów empirycznych i symulacji metodą elementów skończonych. Wyniki kalkulacji opracowanej metody zostały przedstawione jako wykresy obciążenia w funkcji skrócenia oraz momentu w funkcji kąta ugięcia dla różnych wartości mimośrodu siły ściskającej. Nośności profili były obliczane dzięki zastosowaniu analizy krzywej załomów plastycznych, obliczeń numerycznych metodą elementów skończonych, wyników empirycznych oraz obliczeń analitycznych w oparciu o normę EN 1993-1-3. Rezultaty wszystkich obliczeń zestawiono i porównano ze sobą.

Received: 2025-09-05, Revised: 2026-02-07